ACS APPLIED MATERIALS & INTERFACES

Research Article

www.acsami.org

Preparation of a Superhydrophobic and Peroxidase-like Activity Array Chip for H_2O_2 Sensing by Surface-Enhanced Raman Scattering

Zhi Yu,[†,‡] Yeonju Park,[‡] Lei Chen,[⊥] Bing Zhao,[§] Young Mee Jung,*[,‡] and Qian Cong*[,†]

[†]Key Laboratory for Bionic Engineering of Ministry of Education, Jilin University, Changchun 130025, China

[‡]Department of Chemistry, Institute for Molecular Science and Fusion Technology, Kangwon National University, Chunchon 200-701, Korea

[⊥]Key Laboratory of Preparation and Applications of Environmental Friendly Materials, Ministry of Education, Jilin Normal University, Siping 136000, P. R. China

[§]State Key Laboratory of Supramolecular Structure and Materials, Jilin University, Changchun 130012, P. R. China

Supporting Information

ABSTRACT: In this paper, we propose a novel and simple method for preparing a dual-biomimetic functional array possessing both superhydrophobic and peroxidase-like activity that can be used for hydrogen peroxide (H_2O_2) sensing. The proposed method is an integration innovation that combines the above two properties and surface-enhanced Raman scattering (SERS). We integrated a series of well-ordered arrays of Au points (d = 1 mm) onto a superhydrophobic copper (Cu)/silver (Ag) surface by replicating an arrayed molybdenum template. Instead of using photoresists and the traditional lithography method, we utilized a chemical etching method (a substitution reaction between Cu and $HAuCl_4$) with a Cu/Ag superhydrophobic surface as the barrier layer, which has the benefit of water repellency. The as-prepared Au points were observed to possess peroxidase-like activity, allowing for catalytic oxidation of the chromogenic molecule *o*-phenylenediamine dihydrochloride (OPD). Oxidation was evidenced by a color change in the presence of H_2O_2, which allows the array chip to act as an H_2O_2 sensor. In this study, the water repellency of the superhydrophobic surface was used to fabricate the array chip and increase the local reactant concentration during the catalytic reaction. As a result, the catalytic reaction occurred when only 2 μL of an aqueous sample (OPD/H_2O_2) was placed onto the Au point, and the enzymatic product, 2,3-diaminophenazine, showed a SERS signal distinguishable from that of OPD after mixing with 2 μL of colloidal Au. Using the dual-biomimetic functional array chip, quantitative analysis of H_2O_2 was performed by observing the change in the SERS spectra, which showed a concentration-dependent behavior for H_2O_2. This method allows for the detection of H_2O_2 at concentrations as low as 3 pmol per 2 μL of sample, which is a considerable advantage in H_2O_2 analysis. The as-prepared substrate was convenient for H_2O_2 detection because only a small amount of sample was required in each analysis. Highly sensitive detection was realized using SERS. Therefore, this chip was shown to exhibit significant potential for applications in bioanalysis.

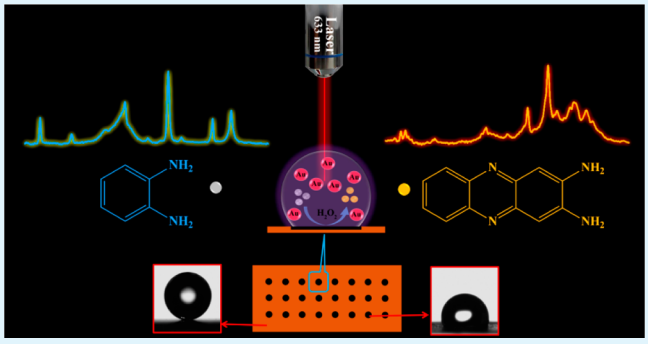

KEYWORDS: *dual-biomimetic functional, superhydrophobic, peroxidase-like activity, H_2O_2 quantitative analysis, surface-enhanced Raman spectroscopy*

1. INTRODUCTION

Biomimetic materials with superhydrophobic surfaces, which have water contact angles (CAs) greater than 150°, are extremely important for various applications.[1,2] This topic has aroused considerable interest because of its potential benefits to daily life and many industrial processes. Various phenomena, such as snow sticking, contamination, oxidation, and current conduction, are expected to be inhibited on such a surface.[3−6] Many elegant methods have been developed for the construction of micro- and nanostructures for superhydrophobic surfaces, such as laser ablation and photolithography-based microfabrication,[7−9] solidification of melted alkyl ketene dimers,[10] microwave-plasma-enhanced chemical vapor deposition of trimethoxylmethoxysilane,[11] phase separation,[12] domain-selective oxygen plasma treatment,[13] and sol−gel methods.[14] Low-surface-energy materials, such as fluoroalkylsilane and alkylsulfhydryl, are needed to prepare superhydrophobic surfaces following the construction of micro- and nanostructures. The superhydrophobic/hydrophobic property could also be used for the fabrication of other materials

Received: June 21, 2015
Accepted: October 5, 2015
Published: October 5, 2015

DOI: 10.1021/acsami.5b08643
ACS Appl. Mater. Interfaces 2015, 7, 23472−23480

because it can prevent water from adhering to the surface; for instance, paper microfluidic chips[15−17] have been prepared using a hydrophobic photoresist to replicate the pattern of the template.

Another attractive biomimetic material is biomimetic enzymes, which exhibit enzymatic properties.[18,19] Biological enzyme-mimetic materials have attracted increased attention in recent years. Yan and co-workers first reported that Fe_3O_4 nanoparticles exhibit intrinsic peroxidase-like activity, which can catalyze chromogenic substrates, resulting in a color change in the presence of hydrogen peroxide (H_2O_2).[20] Their work opened the door for the development of nanomaterials that possess enzyme-mimetic properties. Since then, numerous new types of enzyme-mimetic materials have been developed, including polymer-coated CeO_2 nanoparticles,[21] single- and multiple-wall carbon nanotubes,[22] $BiFeO_3$ nanoparticles,[23] graphene oxide,[24] and positively charged gold (Au) nanoparticles.[25] These materials overcome the disadvantages of natural enzymes and exhibit excellent performance in the colorimetric detection of H_2O_2. H_2O_2 is a simple compound in nature but has great importance in pharmaceutical, clinical, environmental, mining, textile, and food manufacturing applications.[26,27] In living organisms, in addition to its well-known cytotoxic effects, H_2O_2 also plays an essential role as a signaling molecule in regulating diverse biological processes, such as immune-cell activation, vascular remodeling, apoptosis, stomatal closure, and root growth.[28−30] Therefore, detection of H_2O_2 is of great importance. In addition, H_2O_2 is a byproduct of several classical biochemical reactions that are catalyzed by enzymes, such as glucose oxidase (GOx) and alcohol oxidase (AlOx). As a result, H_2O_2 can be used as a biomarker of these types of enzymatic reactions. Therefore, H_2O_2 detection is important in both theory and practical study.

A variety of quantitative methods for determination of H_2O_2, such as titrimetric,[31] fluorescence,[32−34] and electrochemical,[35] have already been developed and are commonly used. Titrimetric analysis uses a simple apparatus but has low sensitivity. Fluorescence methods have been extensively developed because they benefit from a low detection limit. However, these methods require expensive reagents (such as fluorescence tags) and are time-consuming. Electrochemical methods have also been reported. In these methods, determination of H_2O_2 relies on direct oxidation of the molecule using metal electrodes, such as a platinum electrode in a supporting electrolyte[35] or a copper (Cu) electrode by direct catalytic reduction.[36] These systems do not always offer optimal conditions for H_2O_2 detection because of their poor selectivity, low sensitivity, and electrode fouling.[37−40] Another electrochemical method based on modification of the electrodes with enzymes was proposed. This method shows higher selectivity and sensitivity than electrochemical methods that rely on direct oxidation of the molecule. However, this method employs enzymes that are unstable and expensive as reagents, and electrode modification is a barrier to practical application.[41,42]

In comparison, enzymatic reactions (e.g., the horseradish peroxidase (HRP)−H_2O_2 enzymatic reaction system) show high substrate specificities and high efficiency under mild conditions for biological catalysis, which enables their significant practical application in medicine, the chemical industry, food processing, and agriculture.[43] The enzymatic reaction has been used to fabricate various detection sensors. For example, a single nanochannel system with walls that were decorated with covalently linked HRP has been reported for quantitative H_2O_2 analysis.[44] This method shows high selectivity and sensitivity and can be used multiple times without losing sensitivity. However, natural enzymes suffer from several serious disadvantages, such as denaturation by environmental changes, digestion by proteases, and time-consuming and expensive preparation and purification processes, which limit their application.[45,46] As a result, the enzyme mimetics are superior for H_2O_2 analysis.

Surface-enhanced Raman scattering (SERS) has been utilized for many applications, such as bioanalysis, single-molecule detection, and characterization of compounds and materials. This versatility is attributed to the many advantages of SERS, such as its rapidity, ultrasensitivity, and high selectivity.[47−50] SERS also possesses the important advantages of detecting materials at low concentrations or at the submonolayer coverage limit using a minimal sample volume. Additionally, the chromogenic substrate always exhibits excellent Raman activity in enzymatic reactions and can produce strong SERS signals after mixing with noble-metal nanoparticles.[51,52] In our previous study, SERS was introduced into the enzyme-linked immunosorbent assay as a detection tool, and detection of the human cardiac isoform of troponin T was realized based on the enhanced SERS signal of the enzymatic product 3,3′,5,5′-tetramethylbenzidine(2+).[53] This method introduced a new application for SERS and expanded the list of analytical tools utilized in clinical diagnostics.

Here, for the first time, we report a facile, cost-effective, and environmentally friendly method for the fabrication of a novel dual-biomimetic functional (superhydrophobic and peroxidase-like activity) material, which can be used for H_2O_2 analysis (Scheme 1) based on SERS. We utilized the water repellency of the superhydrophobic surfaces as a barrier layer for chemical etching to integrate a series of Au array points onto the superhydrophobic surface. This approach improves upon the use of a photoresist in traditional lithography. The as-prepared Au array points possess HRP-like properties and can catalytically oxidize the chromogenic molecule *o*-phenylenediamine dihydrochloride (OPD) in the presence of H_2O_2, resulting in a color change. Therefore, the as-prepared dual-biomimetic functional substrate can be successfully used for H_2O_2 sensing. Quantitative analysis of H_2O_2 was performed by placing the test

Scheme 1. Preparation of the Dual-Biomimetic Functional Array Chip

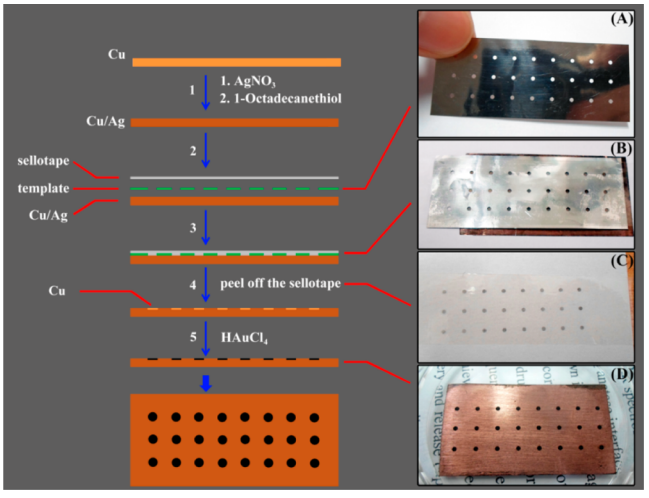

DOI: 10.1021/acsami.5b08643
ACS Appl. Mater. Interfaces 2015, 7, 23472−23480

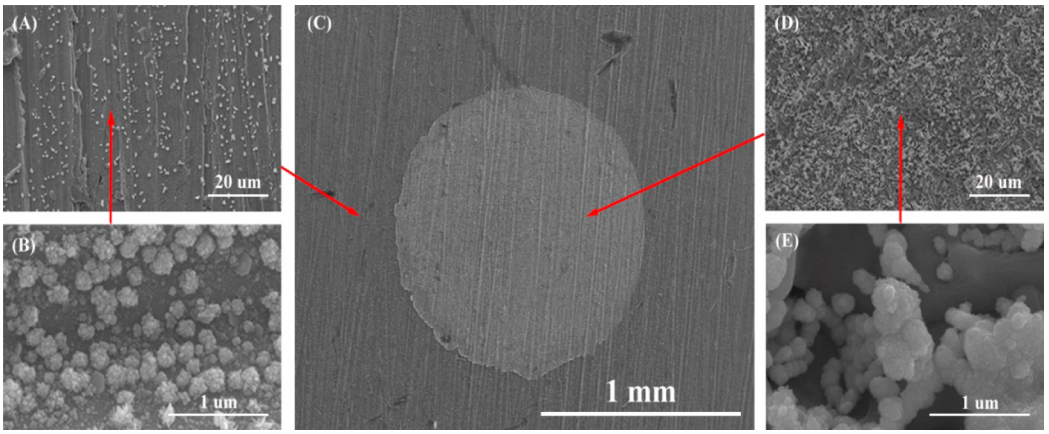

Figure 1. SEM images of the area surrounding the Cu/Au point (A), the amplified image of A (B), the entire graphic of the Cu/Au point (C), the inner portion of the point (D), and the amplified image of D (E).

sample (OPD−H_2O_2) onto the active points (the points exhibiting hydrophilic properties) of the chip where the enzymatic reaction occurs. SERS was then used as a detection tool by placing a droplet of Au colloid onto the test sample, and the distinctive SERS spectrum of the enzymatic product was obtained. Furthermore, a quantitative analysis plot based on the concentration-dependent SERS spectra clearly displays good linearity from 10^{-3} to 10^{-6} mol/L and a detection limit as low as 10^{-6} mol/L. The as-prepared dual-biomimetic functional substrate exhibits several advantages. First, the water repellency of the superhydrophobic surface allows it to be utilized as a barrier layer instead of the photoresist used in traditional lithography. This technique simplifies the etching process and reduces the cost. Second, only the Au array points possess hydrophilic properties, whereas the other parts of the chip exhibit water repellency. This character localizes the reaction solution on the Au points, which promotes the enzymatic reaction that occurs in the presence of H_2O_2. The array chip can be used as a reaction vessel. Third, only 2 μL of the reaction solution was used during the reaction, which allows for a rapid trace analysis using SERS. These results indicate that this dual-biomimetic functional array chip shows significant potential in bioanalysis.

2. EXPERIMENTAL SECTION

2.1. Materials. *o*-Phenylenediamine dihydrochloride (OPD), 3,3′,5,5′-tetramethylbenzidine (TMB), hydrogen peroxide (H_2O_2) solution (30 wt % water), silver nitrate ($AgNO_3$), gold(III) chloride trihydrate ($HAuCl_4{\cdot}3H_2O$), 1-octadecanethiol, ethanol [200 proof, high-performance liquid chromatography (HPLC)/spectrophotometric grade], and trisodium citrate were purchased from Sigma-Aldrich Ltd. (St. Louis, MO) at the highest purity available and were used as received, without further purification. A molybdenum (Mo) template [27 array holes (3 × 9), d = 1 mm, and 50 mm × 20 mm × 30 μm] was purchased from Beijing Xinxing Brain Technology Co. Ltd., China. A Cu sheet (100 mm × 100 mm, ≥99.9%) was purchased from the Tianjin Guangfu Fine Chemical Research Institute in China. A blood sample with an H_2O_2 concentration of 3.5 × 10^{-6} M was supported by the Department of Basic Medical Sciences at Jilin University, P. R. China. Deionized and ultrapure water (18.0 MΩ/cm) were used throughout the study.

2.2. Preparation of the Superhydrophobic Surface. The Cu sheet was cut into 20 mm × 40 mm sections and then polished with abrasive paper to remove the surface oxide layer. After polishing, the Cu substrate was ultrasonically cleaned with ethanol, followed by deionized water. After drying under a N_2 flow, the Cu sheet was immersed in a 1 × 10^{-3} mol/L aqueous $AgNO_3$ solution at ambient temperature for 1 min. After thorough rinsing with deionized water, the sheet was immersed in a 1 × 10^{-3} mol/L 1-octadecanethiol solution overnight (step 1 in Scheme 1).

2.3. Integration of the Au Point onto the Superhydrophobic Surface. Scotch tape was pasted onto the as-prepared superhydrophobic surface with the Mo template as a barrier layer. The Scotch tape was then slightly pressed with tweezers in places where there were holes (steps 2 and 3 in Scheme 1). Next, the Scotch tape and Mo template were peeled off together to remove the silver (Ag) layer on the surface within the point field (step 4 in Scheme 1). Then, the substrate was immersed in a 1% $HAuCl_4$ solution for 1 min, followed by washing and drying steps (step 5 in Scheme 1).

2.4. Characterization of the Peroxidase-like Property by UV−Visible (UV−Vis) Spectroscopy. OPD (10^{-3} mol/L) and TMB (10^{-3} mol/L) were used to verify the peroxidase-like property of the Au displaced by Cu substrate. First, the Cu/Au complex was directly prepared by immersing a Cu sheet (after polishing and washing) into a 10^{-3} mol/L $HAuCl_4$ solution for 1 min, followed by washing with water and drying with N_2 gas. The Cu/Au complex was cut into 5 mm × 5 mm samples. A Cu sheet without Au modification was also cut into 5 mm × 5 mm samples for comparison. As-prepared substrate samples were placed in centrifuge tubes (1 mL), and then 500 μL of OPD (TMB) and 500 μL of 1% H_2O_2 were added. The UV−vis spectra were collected after 10 min.

2.5. Concentration-Dependent UV−Vis Spectra. H_2O_2 was diluted to the following concentrations: 10^{-2}, 10^{-3}, 10^{-4}, 10^{-5}, 10^{-6}, 10^{-7}, and 0 mol/L. OPD (10^{-3} mol/L, 500 μL) and H_2O_2 (1%, 500 μL) were added to the centrifuge tube (1 mL) with a sample of the 5 mm × 5 mm Cu/Au complex. The UV−vis spectra were collected after 10 min under ambient temperature.

2.6. Preparation of Au Nanoparticles. Au nanoparticles were prepared as follows: 1 mL of a $HAuCl_4$ solution (1%, w/v) was added to 99 mL of ultrapure water. After boiling, 4 mL of a trisodium citrate solution (1%, w/v) was added, and the solution was boiled for 15 min. The Au colloid exhibited a maximum absorption at 520 nm with an average diameter of 20 nm.[54]

2.7. SERS Measurement Based on the Dual-Biomimetic Functional Array Chip. OPD (10^{-3} mol/L, 500 μL) and H_2O_2 (0, 10^{-7}, 10^{-6}, 10^{-5}, 10^{-4}, 10^{-3}, and 10^{-2} mol/L, 500 μL) were first mixed together in a tube. The resulting solution was then placed onto the Au points of the array chip. After 10 min, 2 μL of the Au colloid was placed onto each point to mix with the solution, and the SERS spectrum of the droplet on each point was collected.

2.8. Characterization and Measurements. SERS spectra were measured using a Jobin Yvon/Horiba LabRam ARAMIS Raman spectrometer with radiation from an air-cooled HeNe laser (633 nm). Raman scattering was detected at a geometry of 180° using a Peltier/thermoelectric-cooled (−70 °C) charge-coupled-device camera (1024 × 256 pixels[2]). The typical accumulation time used in this study was 10 s. The UV−vis spectra of the enzyme product were obtained on a

DOI: 10.1021/acsami.5b08643
ACS Appl. Mater. Interfaces 2015, 7, 23472−23480

PDA UV−vis spectrophotometer, S-3100 series (SCINCO). Scanning electron microscopy (SEM) images were recorded on a field-emission scanning electron microscope, S-4300 series (Hitachi, Japan). The CAs of 4 μL drops were measured using a CA meter (JC2000A) and interface tension/CA measurement equipment (Powereach, China) at ambient temperature.

3. RESULTS AND DISCUSSION

3.1. Fabrication and Characterization of the Superhydrophobic Surface. All of the preparation steps for the substrate are listed in Scheme 1. After polishing, the Cu sheet only possesses microstructures with striped shapes, as shown in Figure 1A,C, which is not sufficient for preparing the superhydrophobic surface. Therefore, the Cu sheet was immersed in a 10^{-3} mol/L $AgNO_3$ solution, and a substitution reaction occurred between Cu and Ag^+ because Cu is more active than Ag. The reaction proceeded as follows:

$$Cu + 2Ag^+ \rightarrow Cu^{2+} + 2Ag$$

As a result, Ag nanoparticles were generated on the Cu surface, and the surface morphology was characterized by SEM, as shown in Figure 1A,B. As shown in Figure 1, Ag nanoparticles aggregated into a nanocluster on the Cu surface; thus, the surface possesses both micro- and nanostructures.

However, the surface was not yet superhydrophobic because the CA was only 114° (Figure 2A). Figure 2B shows an image of a water droplet suspended from a Cu/Ag substrate that was turned over. Thus, the surface possesses high adhesion properties because water remains on the surface even when the substrate is turned over.

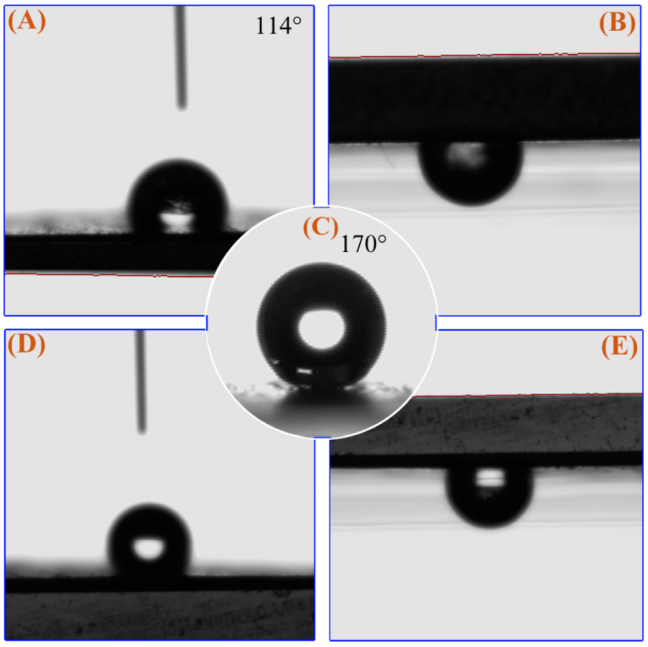

Figure 2. CA of the Cu/Ag substrate before modification with 1-octadecanethiol (A), the Cu/Ag substrate before modification with 1-octadecanethiol (turned over) (B), the Cu/Ag substrate after modification with 1-octadecanethiol (C), the Au replaced by Cu (D), and the Au replaced by Cu (turned over) (E).

This observation is a result of the surface free energy not being sufficiently low for the surface to achieve superhydrophobic character. To lower the surface free energy, a 10^{-3} mol/L 1-octadecanethiol solution was used to modify the Cu/Ag surface through the interaction between Ag and −SH groups. Afterward, the surface exhibited excellent superhydrophobic properties, and the CA of the surface achieved a value of 170° (Figure 2C). Moreover, a water droplet rolled away immediately upon coming into contact with the flat superhydrophobic surface (shown in the video in the Supporting Information), indicating the low adhesion properties of the surface. These properties can be used to prevent water from wetting the surface, which can be utilized for the preparation of the array chip.

3.2. Integration and Characterization of the Au Array Point on the Superhydrophobic Surface. First, a piece of Scotch tape was pasted onto the surface of a Mo template with the holes exposed (Scheme 1A, step 2). Then, the template was placed onto the as-prepared superhydrophobic surface so that only the portions of the Scotch tape containing exposed holes were allowed to contact the superhydrophobic surface (Scheme 1B, step 3). After being pressed with tweezers, the Scotch tape could tightly adhere to the superhydrophobic surface. The template and Ag that contacted the Scotch tape were then peeled off the superhydrophobic surface, leaving exposed Cu that matched the template. This portion of the film was partly transformed from superhydrophobic to hydrophilic (step 4). Scheme 1C shows a photograph of the Scotch tape after it was peeled off the template; Ag was pasted onto the Scotch tape as a replicated pattern of the template. The substrate was subsequently immersed in a $HAuCl_4$ solution. The exposed Cu portion reacted with $HAuCl_4$, resulting in the growth of Au on the Cu point (step 5). As indicated in Scheme 1D, the black point (Au) array followed the Mo template, and thus the arrayed Au chip was successfully prepared. An SEM image of a single point is shown in Figure 1C. The photograph indicates that the diameter of the point is approximately 1 mm, which corresponds to the size of the holes on the Mo template. Parts A and B of Figure 1 show SEM images of the outer portion of the Au point, whereas parts C and D of Figure 1 show the inner portion.

The as-prepared Au point also exhibits good water-adhesion properties, as shown in Figure 2D,E. The same conditions as shown for the Cu/Ag surface before modification with 1-octadecanethiol were observed; the water droplet adhered to the surface even when the substrate was turned over.

3.3. Peroxidase-like Activity of the Cu/Au Complex Array Point. Interestingly, the Au points on the as-prepared array chip were found to possess peroxidase-like activity and could catalytically oxidize OPD and TMB in the presence of H_2O_2. However, the Cu sheet without Au also exhibited peroxidase-like activity even though the catalytic efficiency was considerably lower. Accordingly, the improved intrinsic peroxidase-like activity is attributed to the Au on the superhydrophobic surface.

The peroxidase-like activity was first investigated using TMB as a substrate molecule. A 5 mm × 5 mm Cu/Au sheet was used without being integrated into an array chip, and a 5 mm × 5 mm Cu sheet was used as a control experiment. As shown in Figure S1, the Cu/Au sheet catalyzed TMB in the presence of H_2O_2, resulting in a color change from transparent to blue with a maximum absorbance at 652 nm in the UV−vis spectrum.

The reaction mechanism has already been described in our previous work (see Figure S2).[25] Under the same conditions, the Cu sheet led to only a slight change in the solution, yielding a small absorbance band near 400 nm. However, the Cu/Au sheet had no effect on TMB in the absence of H_2O_2, indicating

DOI: 10.1021/acsami.5b08643
ACS Appl. Mater. Interfaces 2015, 7, 23472−23480

that the peroxidase-like activity mainly benefits from the substrate with Au replaced by Cu.

Subsequently, the peroxidase-like activity of the Au was investigated using OPD and a Cu/Au sheet (5 mm × 5 mm) as a test sample and a Cu sheet (5 mm × 5 mm) as a control sample. As shown in Figure 3, the Cu/Au complex can catalytically oxidize OPD with the production of 2,3-diaminophenazine, as indicated by a color change to orange (450 nm). The reaction mechanism is shown in Figure 4.[55−57]

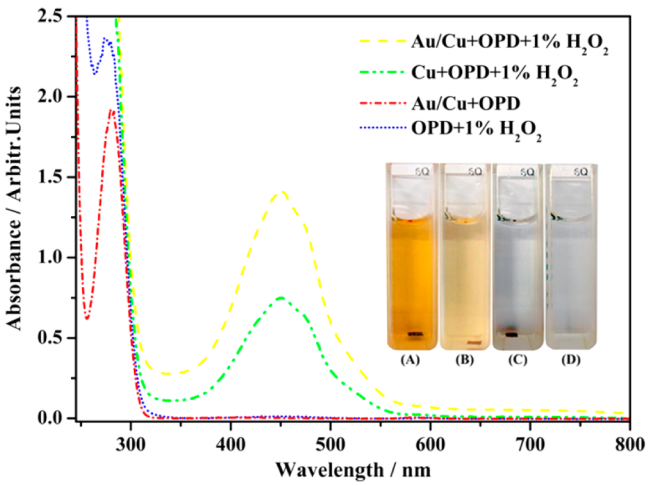

Figure 3. UV−vis spectra of the OPD molecule in the presence of Cu/Au−1% H_2O_2, Cu−1% H_2O_2, Cu/Au, and 1% H_2O_2. The inset images show photographs of these four samples.

Additionally, the Cu sheet also exhibited the same properties, leading to a slight color change of the solution and the same maximum absorbance band at 450 nm. However, on the Au point array chip, only the Au points could contact the reaction solution. Moreover, as previously mentioned, Cu does not have an obvious effect on the catalytic oxidation of TMB in the presence of H_2O_2. Furthermore, as shown in Figure 3, the OPD solutions in the absence of H_2O_2 or the Cu/Au complex exhibit no color change. Therefore, Au displaced by the Cu foil possesses peroxidase-like activity, which can catalytically oxidize TMB and OPD in the presence of H_2O_2. In the further study, we choose not TMB but OPD as a substrate molecule for H_2O_2 quantitative analysis by SERS. This is because the SERS spectra of OPD and the product (2,3-diaminophenazine) show obvious differences (described in the following part), which can ensure the accuracy of quantitative analysis. However, the SERS spectra of the TMB molecule before and after the catalytic reaction (the data not shown in the manuscript) show no obvious differences, which is not appropriate for quantitative analysis of H_2O_2.

Next, we examined the time-dependent catalytic activity of Au for the oxidation of OPD. Figure 5 shows the time-dependent maximum absorbance intensity of OPD at 450 nm in the presence of Cu/Au−H_2O_2, Cu−H_2O_2, H_2O_2, and Cu/Au. The intensity increased over time in the presence of Cu/Au−H_2O_2 and Cu−H_2O_2, whereas the other two samples exhibited no obvious change. However, in the presence of H_2O_2 and Cu/Au only, the intensity of the OPD solution at 450 nm in the presence of H_2O_2 exhibits a slight increase within 10 min and then remains stable (Figure 5).

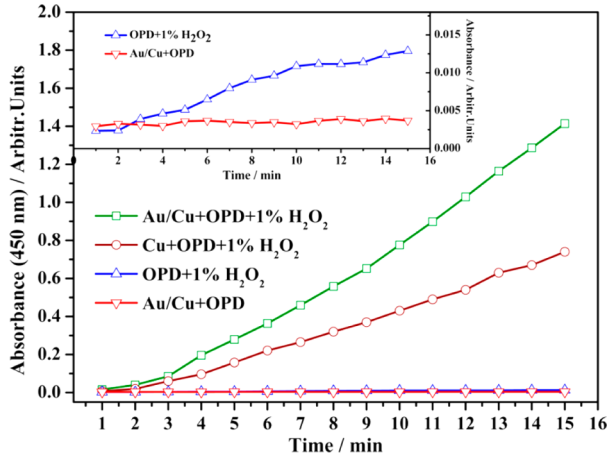

Figure 5. Time-dependent maximum absorbance intensity of OPD at 450 nm in the presence of Cu/Au−H_2O_2, Cu−H_2O_2, H_2O_2, and Cu/Au. The inset shows a magnified view of the figure for H_2O_2 and Cu/Au.

However, this phenomenon can be neglected because the absorbance intensity is not sufficiently high to affect the entire reaction. Next, we examined the concentration-dependent UV−vis spectra for H_2O_2 concentrations ranging from 10^{-2} to 10^{-7} mol/L. Cu/Au sheets (5 mm × 5 mm) were used as the catalyst and immersed in a mixed solution of OPD and H_2O_2 for 10 min. As shown in Figure 6, the intensity of the maximum absorbance band at 450 nm increased with increasing H_2O_2 concentration; thus, Au on the Cu surface exhibits good H_2O_2 responsivity.

3.4. Quantitative Analysis of H_2O_2 Based on the Array Chip Using SERS. Although UV−vis can be used to monitor the concentration change of H_2O_2, this method for

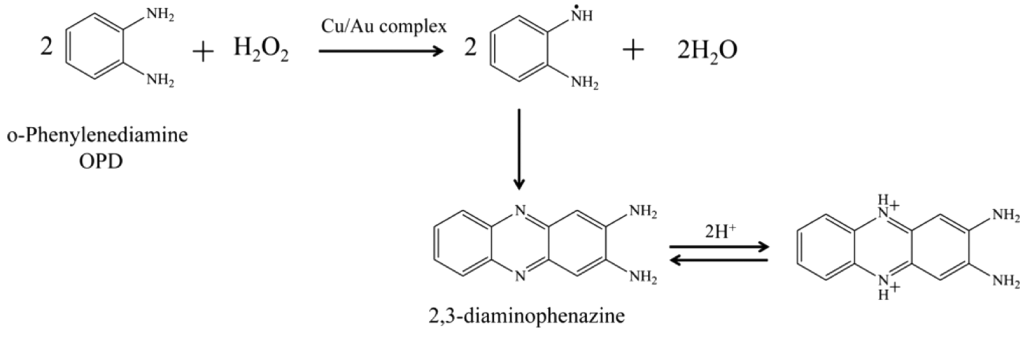

Figure 4. Mechanism of the catalytic reaction of a OPD molecule by the Cu/Au complex.

DOI: 10.1021/acsami.5b08643
ACS Appl. Mater. Interfaces 2015, 7, 23472−23480

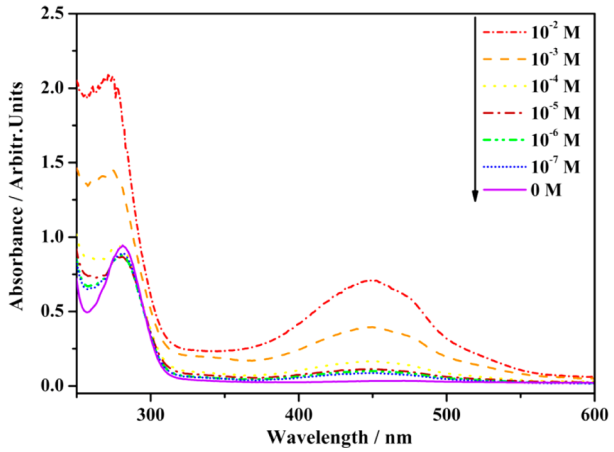

Figure 6. Concentration-dependent UV−vis spectra of the catalytic reaction solutions over the H_2O_2 concentration range of 10^{-2}−10^{-7} mol/L and the blank sample.

quantitatively analyzing H_2O_2 can be further improved by using the as-prepared dual-biomimetic functional array chip with SERS as the detection tool. The combination of the array chip and SERS allows the sample volume to be decreased from 1 mL (UV−vis method) to 2 μL without losing detection sensitivity due to the wetting of the superhydrophobic surface and the greatly enhanced SERS signal from the Au colloid in the measurement. First, we used UV−vis to verify the interaction between the Au colloid and the molecule in the reaction solution with changes in the H_2O_2 concentration. As noted above, the concentration-dependent reaction solution was mixed with the Au colloid at a ratio of 1:1.

As shown in Figure 7, the absorbance band near 700 nm shifted toward shorter wavelengths, and the intensity first

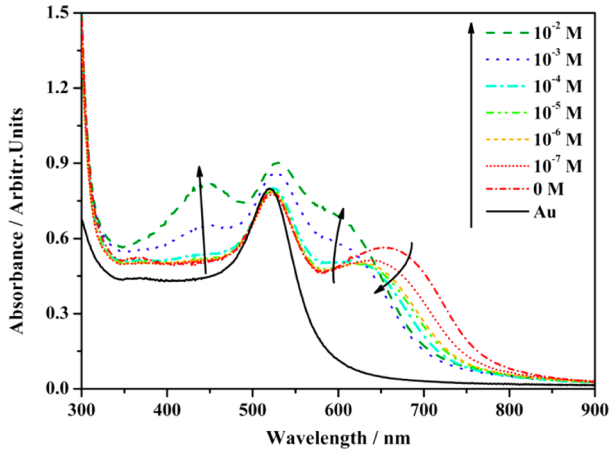

Figure 7. Concentration-dependent UV−vis spectra of the reaction solution with different H_2O_2 concentrations after mixing with the Au colloid in a ratio of 1:1.

decreased and then increased. This observation clearly indicates that both OPD and the enzymatic product (2,3-diaminophenazine) can lead to aggregation of the Au colloid, which occurred predictably with increasing H_2O_2 concentration. These results also indicate that the content of OPD decreased, whereas that of the enzymatic product (2,3-diaminophenazine) increased. In addition, the results indicate that the Au colloid could interact with both OPD and the enzymatic product.

Subsequently, the as-prepared dual-biomimetic functional array chip was used as a reaction plate on which the catalytic reaction proceeded with only a 2 μL droplet containing a mixture of OPD and H_2O_2 [1:1 (v/v)]. Because of the superhydrophobic properties of the substrate, the droplet can be concentrated at the Au point for the catalytic reaction. After 10 min, 2 μL of the Au colloid was mixed with the reaction solution, and the SERS signal of the solution was recorded.

Figure 8 compares the SERS signals of OPD and the product (2,3-diaminophenazine), revealing that the SERS signal of the

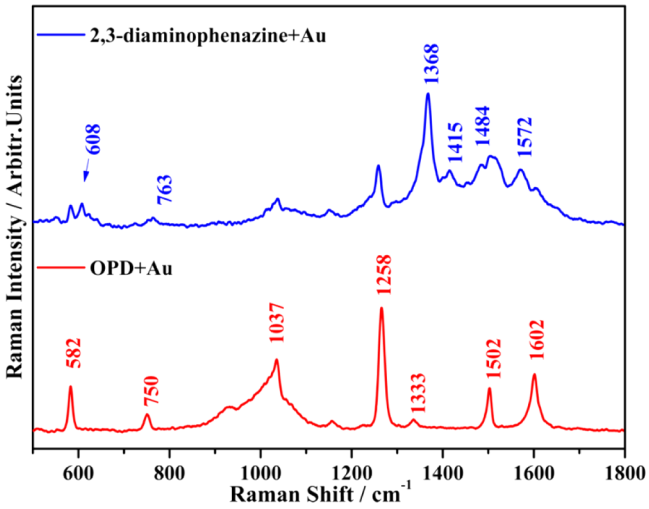

Figure 8. SERS spectra of OPD and the product 2,3-diaminophenazine.

molecule changed significantly after the catalytic reaction. Several new bands belonging to 2,3-diaminophenazine appeared at 608, 763, 1368, 1415, 1484, and 1572 cm^{-1}, whereas the intensity of the bands at 582, 1037, 1258, and 1602 cm^{-1}, which were attributed to OPD, decreased. The assignments of the main bands are listed in Table 1.[57−61]

Subsequently, the concentration-dependent SERS signal of the catalytic reaction solution was collected at H_2O_2 solution concentrations ranging from 10^{-2} to 10^{-7} mol/L. The concentration-dependent SERS spectra in Figure 9 show that the intensities of the bands assigned to 2,3-diaminophenazine

Table 1. Main SERS Band Assignments of OPD and 2,3-Diaminophenazine

SERS/cm^{-1}		
OPD	2,3-diaminophenazine	assignment
582	582	ring deformation
	608	ring deformation
750		C−H wag
	763	ring deformation
1037	1037	ring deformation, ring breathing
1258	1258	C−N stretching in the benzenoid
1333		C−H in-plane bend
	1368	$C-N^+$
	1415	half-oxidized phenazine-like structure
	1484	phenazine-like structure
1502		ring deformation, C−H in-plane bend
	1572	C═N
1602		NH_2 scissor

DOI: 10.1021/acsami.5b08643
ACS Appl. Mater. Interfaces 2015, 7, 23472−23480

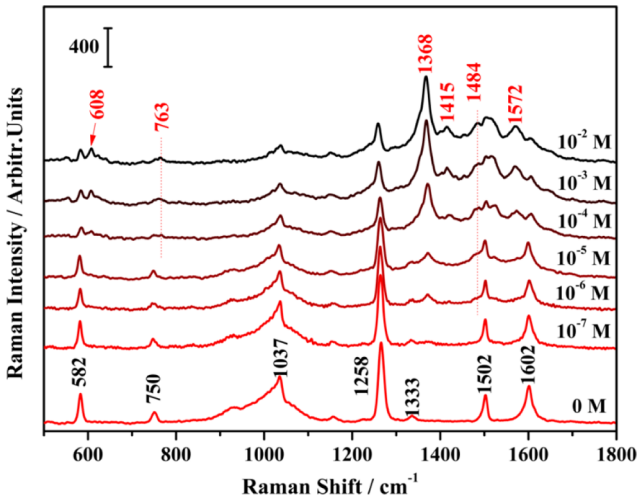

Figure 9. Concentration-dependent SERS spectra of the catalytic reaction solutions with H_2O_2 concentrations ranging from 10^{-2} to 10^{-7} mol/L and the blank sample.

increased with increasing H_2O_2 concentration, whereas those attributed to OPD decreased. The most obvious band at 1368 cm^{-1} was chosen for H_2O_2 quantitative analysis.

Figure 10A shows that the Raman intensity of the band at 1368 cm^{-1}, which was used to verify the detection limit of the method, exists for samples with H_2O_2 concentrations of 0, 10^{-7}, 10^{-6}, 5×10^{-6}, and 10^{-5} mol/L. The error bar indicates three independent measurements, and the threshold line is located at three standard deviations from the value for the blank sample.

In Figure 10A, H_2O_2 is clearly identified from the threshold line even though its concentration is 10^{-6} mol/L, which indicates that the assay allows for the detection of as little as 3 pmol of H_2O_2 per 2 μL of sample. A comparison of our method with other methods[62,63] for the detection of H_2O_2 is summarized in Table S1. The detection limit of our method shows a sensitivity that is similar to or better than other methods. However, the absolute amount of the detection sample of our method is as low as 3 pmol of H_2O_2, which shows a considerable advantage over other methods. For the electrochemical method, the lowest concentration of H_2O_2 that could be detected is similar to our method.[27] However, when we consider the sample amount used in the detection system, only 2 μL of sample is used in our detection system, whereas the sample volume used in other electrochemical methods depends on the size of the electrode. Thus, our detection system shows considerable advantages for H_2O_2 analysis.

The intensity of the band at 1368 cm^{-1} was then chosen to plot the calibration curves to be used for quantitative analysis of H_2O_2. The intensity of the band at 1368 cm^{-1} versus the logarithm of the H_2O_2 concentration is plotted over the concentration range from 10^{-3} to 10^{-6} mol/L (Figure 10B). The error bars indicate the batch-to-batch variability of the SERS intensity from three independent measurements. The SERS intensity versus the logarithm value of the H_2O_2 concentration is linear ($Y = -252.40X + 1621.04$; $R^2 = 0.9918$), where Y represents the SERS intensity of the band at 1368 cm^{-1} for 2,3-diaminophenazine and X is the H_2O_2 concentration. Consequently, the concentration-dependent SERS spectra could be successfully used for quantitative analysis of H_2O_2. For practical applications, blood samples with H_2O_2 concentrations of 3.5×10^{-6} M were determined using the plotted standard curve ($Y = -252.40X + 1621.04$) in Figure 10. H_2O_2 samples at two different concentrations (2.68×10^{-5} and 5.18×10^{-5} M) were prepared by adding extraneous H_2O_2 (5×10^{-5} M and 10^{-4} M) into each of the blood samples (3.5×10^{-6} M) with a volume ratio of 1:1. SERS spectra of these two samples were then measured. As shown in Table S2, the average recoveries of these three concentrations determined by this method were 99.06%, 100.5%, and 99.37%, respectively. The relative standard deviations of three independent detections for three different concentration samples were 0.07936, 0.04031, and 0.0095, respectively (Table S2). The proposed method for detection of H_2O_2 is an accurate analytical method with good repeatability and reproducibility.

4. CONCLUSION

In this study, based on the idea of integration innovation, we integrated Au points, which exhibit peroxidase-like activity, onto a Cu/Ag superhydrophobic surface to fabricate a dual-biomimetic functional substrate. The synergy of these two functions was fully reflected in the trace analysis of H_2O_2. During quantitative analysis of H_2O_2, the superhydrophobic properties can be used to decrease the sample volume to only 2 μL of the reaction solution. Additionally, when a 2 μL sample was placed onto an Au point, a catalytic reaction occurred that oxidized OPD to 2,3-diaminophenazine as a result of the peroxidase-like activity of the Au point. The concentration-dependent SERS spectra, collected by adding 2 μL of colloidal Au to the reaction solution, changed predictably with a change

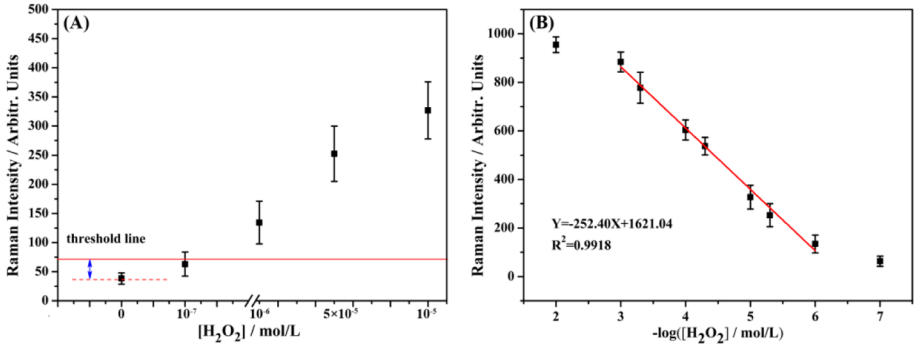

Figure 10. (A) SERS intensities of the H_2O_2 samples with concentrations of 0, 10^{-7}, 10^{-6}, 5×10^{-6}, and 10^{-5} mol/L, where the threshold line indicates 3 standard deviations from the value of the blank sample. (B) Quantitative analysis plot showing the intensity of the peak at 1368 cm^{-1} versus the logarithm value of the H_2O_2 concentration. The error bar indicates three independent measurements.

DOI: 10.1021/acsami.5b08643
ACS Appl. Mater. Interfaces 2015, 7, 23472−23480

in the H_2O_2 concentration. For further analysis, a quantitative plot was built using the intensity of the band at 1368 cm^{-1} versus the logarithm of the H_2O_2 concentration. This plot exhibited good linearity in the range of 10^{-3}–10^{-6} mol/L, and the detection limit was as low as 10^{-6} mol/L (3 pmol per 2 μL). This study proposed a simple, low-cost, and convenient method for the preparation of novel dual-biomimetic functional array chips, and the introduction of SERS further improved the utility of the substrate.

■ ASSOCIATED CONTENT

Supporting Information

The Supporting Information is available free of charge on the ACS Publications website at DOI: 10.1021/acsami.5b08643.

video of a water droplet coming into contact with the flat superhydrophobic surface (AVI)

UV–vis spectra of the TMB molecule in the presence of Cu/Au–1% H_2O_2, Cu–1% H_2O_2, and Cu/Au (Figure S1), mechanism of the catalytic reaction of TMB (Figure S2), DLS spectra of Au, Au with 2,3-diaminophenazine, and Au with OPD (Figure S3), SERS spectra of the mixing solution of OPD and H_2O_2 as a function of the mixing time (Figure S4), detection level of H_2O_2 assays (Table S1), and summary of SERS spectra of the blood samples (Table S2) (PDF)

■ AUTHOR INFORMATION

Corresponding Authors

*E-mail: ymjung@kangwon.ac.kr (Y.M.J.).

*E-mail: congqian@jlu.edu.cn (Q.C.).

Notes

The authors declare no competing financial interest.

■ ACKNOWLEDGMENTS

The research was supported by the National Natural Science Foundation of P. R. China (Grants 21273091 and 21221063), the Specialized Research Fund for the Doctoral Program of Higher Education (Grant 20110061110017), the 111 project (B06009), and the Development Program of the Science and Technology of Jilin Province (Grant 20110338). This work was also supported by a National Research Foundation of Korea grant funded by the Ministry of Science, ICT and Future Planning (Grant 2014K2A2A2000713) and by a research grant from the Agency for Defense Development. The authors thank the Central Laboratory of Kangwon National University for the measurements of Raman spectra.

■ REFERENCES

(1) Wang, R.; Hashimoto, K.; Fujishima, A.; Chikuni, M.; Kojima, E.; Kitamura, A.; Shimohigoshi, M.; Watanabe, T. Light-induced Amphiphilic Surfaces. *Nature* **1997**, *388*, 431–432.

(2) Sun, T.; Feng, L.; Gao, X.; Jiang, L. Bioinspired Surfaces with Special Wettability. *Acc. Chem. Res.* **2005**, *38*, 644–652.

(3) Chen, W.; Fadeev, A. Y.; Hsieh, M. C.; Öner, D.; Youngblood, J.; McCarthy, T. J. Ultrahydrophobic and Ultralyophobic Surfaces: Some Comments and Examples. *Langmuir* **1999**, *15*, 3395–3399.

(4) Feng, L.; Li, S.; Li, Y.; Li, H.; Zhang, L.; Zhai, J.; Song, Y.; Liu, B.; Jiang, L.; Zhu, D. Super-Hydrophobic Surfaces: From Natural to Artificial. *Adv. Mater.* **2002**, *14*, 1857–1860.

(5) Blossey, R. Self-cleaning Surfaces-virtual Realities. *Nat. Mater.* **2003**, *2*, 301–306.

(6) Lafuma, A.; Quéré, D. Superhydrophobic States. *Nat. Mater.* **2003**, *2*, 457–460.

(7) He, B.; Patankar, N. A.; Lee, J. Multiple Equilibrium Droplet Shapes and Design Criterion for Rough Hydrophobic Surfaces. *Langmuir* **2003**, *19*, 4999–5003.

(8) Extrand, C. W. Model for Contact Angles and Hysteresis on Rough and Ultraphobic Surfaces. *Langmuir* **2002**, *18*, 7991–7999.

(9) Bico, J.; Marzolin, C.; Quéré, D. Pearl drops. *Europhys. Lett.* **1999**, *47*, 220–226.

(10) Onda, T.; Shibuichi, S.; Satoh, N.; Tsujii, K. Super-Water-Repellent Fractal Surfaces. *Langmuir* **1996**, *12*, 2125–2127.

(11) Wu, Y.; Sugimura, H.; Inoue, Y.; Takai, O. Thin Films with Nanotextures for Transparent and Ultra Water-Repellent Coatings Produced from Trimethylmethoxysilane by Microwave Plasma CVD. *Chem. Vap. Deposition* **2002**, *8*, 47–50.

(12) Erbil, H. Y.; Demirel, A. L.; Avci, Y.; Mert, O. Transformation of a Simple Plastic into a Superhydrophobic Surface. *Science* **2003**, *299*, 1377–1380.

(13) Teshima, K.; Sugimura, H.; Inoue, Y.; Takai, O.; Takano, A. Ultra-Water-Repellent Poly(ethylene terephthalate) Substrates. *Langmuir* **2003**, *19*, 10624–10627.

(14) Shirtcliffe, N. J.; McHale, G.; Newton, M. I.; Perry, C. C. Intrinsically Superhydrophobic Organosilica Sol–Gel Foams. *Langmuir* **2003**, *19*, 5626–5631.

(15) Abadian, A.; Jafarabadi-Ashtiani, S. Paper-based Digital Microfluidics. *Microfluid. Nanofluid.* **2014**, *16*, 989–995.

(16) Dungchai, W.; Chailapakul, O.; Henry, C. S. Electrochemical Detection for Paper-Based Microfluidics. *Anal. Chem.* **2009**, *81*, 5821–5826.

(17) Godino, N.; Gorkin, R., III; Bourke, K.; Ducrée, J. Fabricating Electrodes for Amperometric Detection in Hybrid Paper/Polymer Lab-on-a-chip Devices. *Lab Chip* **2012**, *12*, 3281–3284.

(18) Song, Y.; Wei, W.; Qu, X. Colorimetric Biosensing Using Smart Materials. *Adv. Mater.* **2011**, *23*, 4215–4236.

(19) Luo, W.; Zhu, C.; Su, S.; Li, D.; He, Y.; Huang, Q.; Fan, C. Self-Catalyzed, Self-Limiting Growth of Glucose Oxidase-Mimicking Gold Nanoparticles. *ACS Nano* **2010**, *4*, 7451–7458.

(20) Gao, L.; Zhuang, J.; Nie, L.; Zhang, J.; Zhang, Y.; Gu, N.; Wang, T.; Feng, J.; Yang, D.; Perrett, S.; Yan, X. Intrinsic Peroxidase-like Activity of Ferromagnetic Nanoparticles. *Nat. Nanotechnol.* **2007**, *2*, 577–583.

(21) Asati, A.; Santra, S.; Kaittanis, C.; Nath, S.; Perez, J. M. Oxidase-Like Activity of Polymer-Coated Cerium Oxide Nanoparticles. *Angew. Chem., Int. Ed.* **2009**, *48*, 2308–2312.

(22) Luo, W.; Li, Y.; Yuan, J.; Zhu, L.; Liu, Z.; Tang, H.; Liu, S. Ultrasensitive Fluorometric Determination of Hydrogen Peroxide and Glucose by Using Multiferroic BiFeO3 Nanoparticles as a Catalyst. *Talanta* **2010**, *81*, 901–907.

(23) Song, Y.; Wang, X.; Zhao, C.; Qu, K.; Ren, J.; Qu, X. Label-Free Colorimetric Detection of Single Nucleotide Polymorphism by Using Single-Walled Carbon Nanotube Intrinsic Peroxidase-Like Activity. *Chem. - Eur. J.* **2010**, *16*, 3617–3621.

(24) Song, Y.; Qu, K.; Zhao, C.; Ren, J.; Qu, X. Graphene Oxide: Intrinsic Peroxidase Catalytic Activity and Its Application to Glucose Detection. *Adv. Mater.* **2010**, *22*, 2206–2210.

(25) Jv, Y.; Li, B.; Cao, R. Positively-charged Gold Nanoparticles as Peroxidiase Mimic and Their Application in Hydrogen Peroxide and Glucose Detection. *Chem. Commun.* **2010**, *46*, 8017–8019.

(26) Tsiafoulis, C. G.; Trikalitis, P. N.; Prodromidis, M. I. Synthesis, Characterization and Performance of Vanadium Hexacyanoferrate as Electrocatalyst of H_2O_2. *Electrochem. Commun.* **2005**, *7*, 1398–1404.

(27) Chen, W.; Cai, S.; Ren, Q.; Wen, W.; Zhao, Y. Recent Advances in Electrochemical Sensing for Hydrogen Peroxide: a Review. *Analyst* **2012**, *137*, 49–58.

(28) Geiszt, M.; Leto, T. L. The Nox Family of NAD(P)H Oxidases: Host Defense and Beyond. *J. Biol. Chem.* **2004**, *279*, 51715–51718.

(29) Giorgio, M.; Trinei, M.; Migliaccio, E.; Pelicci, P. G. Hydrogen Peroxide: a Metabolic By-product or a Common Mediator of Ageing Signals? *Nat. Rev. Mol. Cell Biol.* **2007**, *8*, 722–728.

(30) Laloi, C.; Apel, K.; Danon, A. Reactive Oxygen Signalling: The Latest News. *Curr. Opin. Plant Biol.* **2004**, *7*, 323–328.

DOI: 10.1021/acsami.5b08643
ACS Appl. Mater. Interfaces 2015, 7, 23472–23480

(31) Klassen, N. V.; Marchington, D.; McGowan, H. C. E. H_2O_2 Determination by the I3- Method and by $KMnO_4$ Titration. *Anal. Chem.* **1994**, *66*, 2921−2925.
(32) Mori, I.; Takasaki, K.; Fujita, Y.; Matsuo, T. Selective and Sensitive Fluorometric Determinations of Cobalt(II) and Hydrogen Peroxide. *Talanta* **1998**, *47*, 631−637.
(33) Jie, N.; Yang, J.; Huang, X.; Zhang, R.; Song, Z. Fluorimetric Determination of Hydrogen Peroxide in Water Using Acetaminophen. *Talanta* **1995**, *42*, 1575−1579.
(34) Wolfbeis, O. S.; Durkop, A.; Wu, M.; Lin, Z. A Europium-Ion-Based Luminescent Sensing Probe for Hydrogen Peroxide. *Angew. Chem., Int. Ed.* **2002**, *41*, 4495−4498.
(35) Harrar, J. E. Controlled-Potential Coulometric Determination of Hydrogen Peroxide. *Anal. Chem.* **1963**, *35*, 893−896.
(36) Somasundrum, M.; Kirtikara, K.; Tanticharoen, M. Amperometric Determination of Hydrogen Peroxide by Direct and Catalytic Reduction at a Copper Electrode. *Anal. Chim. Acta* **1996**, *319*, 59−70.
(37) Moattisirat, D.; Velho, G.; Reach, G. Evaluating in Vitro and in Vivo the Interference of Ascorbate and Acetaminophen on Glucose Detection by a Needle-type Glucose sensor. *Biosens. Bioelectron.* **1992**, *7*, 345−352.
(38) Wang, H. Y.; Mu, S. L. Bioelectrochemical Characteristics of Cholesterol Oxidase Immobilized in a Polyaniline Film. *Sens. Actuators, B* **1999**, *56*, 22−30.
(39) Bokoch, M. P.; Devadoss, A.; Palencsar, M. S.; Burgess, J. D. Steady-state Oxidation of Cholesterol Catalyzed by Cholesterol Oxidase in Lipid Bilayer Membranes on Platinum Electrodes. *Anal. Chim. Acta* **2004**, *519*, 47−55.
(40) Lyon, J. L.; Stevenson, K. J. Picomolar Peroxide Detection Using a Chemically Activated Redox Mediator and Square Wave Voltammetry. *Anal. Chem.* **2006**, *78*, 8518−8525.
(41) Holt, R. E.; Cotton, T. M. Surface-enhanced Resonance Raman and Electrochemical Investigation of Glucose Oxidase Catalysis at a Silver Electrode. *J. Am. Chem. Soc.* **1989**, *111*, 2815−2821.
(42) Yang, M. S.; Chung, F. L.; Thompson, M. Acoustic Network Analysis as a Novel Technique for Studying Protein Adsorption and Denaturation at Surfaces. *Anal. Chem.* **1993**, *65*, 3713−3716.
(43) Nelson, D. L.; Cox, M. M. *Lehninger Principles of Biochemistry*, 4th ed.; W. H. Freeman & Co. Ltd.: New York, 2005; Chapter 6.
(44) Ali, M.; Tahir, M. N.; Siwy, Z.; Neumann, R.; Tremel, W.; Ensinger, W. Hydrogen Peroxide Sensing with Horseradish Peroxidase-Modified Polymer Single Conical Nanochannels. *Anal. Chem.* **2011**, *83*, 1673−1680.
(45) Shoji, E.; Freund, M. S. Potentiometric Sensors Based on the Inductive Effect on the pKa of Poly(aniline): a Nonenzymatic Glucose Sensor. *J. Am. Chem. Soc.* **2001**, *123*, 3383−3384.
(46) Breslow, R. Biomimetic Chemistry and Artificial Enzymes: Catalysis by Design. *Acc. Chem. Res.* **1995**, *28*, 146−153.
(47) Han, X. X.; Kitahama, Y.; Itoh, T.; Wang, C. X.; Zhao, B.; Ozaki, Y. Protein-Mediated Sandwich Strategy for Surface-Enhanced Raman Scattering: Application to Versatile Protein Detection. *Anal. Chem.* **2009**, *81*, 3350−3355.
(48) Gu, G. H.; Suh, J. S. Minimum Enhancement of Surface-Enhanced Raman Scattering for Single-Molecule Detections. *J. Phys. Chem. A* **2009**, *113*, 8529−8532.
(49) Centeno, S. A.; Shamir, J. Surface enhanced Raman scattering (SERS) and FTIR Characterization of the Sepia Melanin Pigment Used in Works of Art. *J. Mol. Struct.* **2008**, *873*, 149−159.
(50) Chang, L.; Ding, Y.; Li, X. Surface Molecular Imprinting onto Silver Microspheres for Surface Enhanced Raman Scattering Applications. *Biosens. Bioelectron.* **2013**, *50*, 106−110.
(51) Guarrotxena, N.; Liu, B.; Fabris, L.; Bazan, G. C. Antitags: Nanostructured Tools for Developing SERS-Based ELISA Analogs. *Adv. Mater.* **2010**, *22*, 4954−4958.
(52) Ruan, C.; Wang, W.; Gu, B. Detection of Alkaline Phosphatase Using Surface-Enhanced Raman Spectroscopy. *Anal. Chem.* **2006**, *78*, 3379−3384.
(53) Yu, Z.; Chen, L.; Wang, Y.; Wang, X.; Song, W.; Ruan, W.; Zhao, B.; Cong, Q. A SERS-Active Enzymatic Product Used for the Quantification of Disease-related Molecules. *J. Raman Spectrosc.* **2014**, *45*, 75−81.
(54) Frens, G. Controlled Nucleation for the Regulation of the Particle Size in Monodisperse Gold Suspensions. *Nature, Phys. Sci.* **1973**, *241*, 20−22.
(55) Fornera, S.; Yazawa, K.; Walde, P. Spectrophotometric Quantification of Lactose in Solution With a Peroxidase-based Enzymatic Cascade Reaction System. *Anal. Bioanal. Chem.* **2011**, *401*, 2307−2310.
(56) Liang, A.; Zhang, N.; Jiang, Z.; Wang, S. A Sensitive Resonance Scattering Spectral Assay for the Determination of Trace H_2O_2 Based on the HRP Catalytic Reaction and Nanogold Aggregation. *J. Fluoresc.* **2008**, *18*, 1035−1041.
(57) Baibarac, M.; Baltog, I.; Smaranda, I.; Scocioreanu, M.; Lefrant, S. Hybrid Organic−inorganic Mmaterials Based on Poly(o-phenylenediamine) and Polyoxometallate Functionalized Carbon Nanotubes. *J. Mol. Struct.* **2011**, *985*, 211−218.
(58) Badawi, H. M.; Förner, W.; Ali, S. A. A Comparative Study of The Infrared and Raman Spectra of Aniline and O-, M-, P-phenylenediamine Isomers. *Spectrochim. Acta, Part A* **2013**, *112*, 388−396.
(59) Li, X.; Huang, M.; Duan, W.; Yang, Y.-L. Novel Multifunctional Polymers from Aromatic Diamines by Oxidative Polymerizations. *Chem. Rev.* **2002**, *102*, 2925−3030.
(60) Ullah, H.; Shah, A. A.; Ayub, K.; Bilal, S. Density Functional Theory Study of Poly(o-phenylenediamine) Oligomers. *J. Phys. Chem. C* **2013**, *117*, 4069−4078.
(61) Jiang, H.; Sun, X.; Huang, M.; Wang, Y.; Li, D.; Dong, S. Rapid Self-Assembly of Oligo(o-phenylenediamine) into One-Dimensional Structures through a Facile Reprecipitation Route. *Langmuir* **2006**, *22*, 3358−3361.
(62) Rhee, S. G.; Chang, T.; Jeong, W.; Kang, D. Methods for Detection and Measurement of Hydrogen Peroxide Inside and Outside of Cells. *Mol. Cells* **2010**, *29*, 539−549.
(63) Lin, L.; Song, X.; Chen, Y.; Rong, M.; Zhao, T.; Wang, Y.; Jiang, Y.; Chen, X. Intrinsic Peroxidase-like Catalytic Activity of Nitrogen-doped Grapheme Quantum Dots and Their Application in the Colorimetric Detection of H_2O_2 and Glucose. *Anal. Chim. Acta* **2015**, *869*, 89−95.

DOI: 10.1021/acsami.5b08643
ACS Appl. Mater. Interfaces 2015, 7, 23472−23480